PHYSICS

10.1126/sciadv.1501438

Direct and cost-efficient hyperpolarization of long-lived nuclear spin states on universal $^{15}N_2$-diazirine molecular tags

Thomas Theis,[1]*† Gerardo X. Ortiz Jr.,[1†] Angus W. J. Logan,[1] Kevin E. Claytor,[2] Yesu Feng,[1‡] William P. Huhn,[3] Volker Blum,[3] Steven J. Malcolmson,[1] Eduard Y. Chekmenev,[4] Qiu Wang,[1]* Warren S. Warren[1,2,5]*

Conventional magnetic resonance (MR) faces serious sensitivity limitations which can be overcome by hyperpolarization methods, but the most common method (dynamic nuclear polarization) is complex and expensive, and applications are limited by short spin lifetimes (typically seconds) of biologically relevant molecules. We use a recently developed method, SABRE-SHEATH, to directly hyperpolarize $^{15}N_2$ magnetization and long-lived $^{15}N_2$ singlet spin order, with signal decay time constants of 5.8 and 23 min, respectively. We find >10,000-fold enhancements generating detectable nuclear MR signals that last for over an hour. $^{15}N_2$-diazirines represent a class of particularly promising and versatile molecular tags, and can be incorporated into a wide range of biomolecules without significantly altering molecular function.

INTRODUCTION

Hyperpolarization enables real-time monitoring of in vitro and in vivo biochemistry

Conventional magnetic resonance (MR) is an unmatched tool for determining molecular structures and monitoring structural transformations. However, even very large magnetic fields only slightly magnetize samples at room temperature and sensitivity remains a fundamental challenge; for example, virtually all MR images are of water because it is the molecule at the highest concentration in vivo. Nuclear spin hyperpolarization significantly alters this perspective by boosting nuclear MR (NMR) sensitivity by four to nine orders of magnitude (*1*–*3*), giving access to detailed chemical information at low concentrations. These advances are beginning to transform biomedical in vivo applications (*4*–*9*) and structural in vitro studies (*10*–*16*).

Current hyperpolarization technology is expensive and associated with short signal lifetimes

Still, two important challenges remain. First, hyperpolarized MR is associated with high cost for the most widespread hyperpolarization technology [dissolution dynamic nuclear polarization (d-DNP), $2 million to $3 million for commercial hyperpolarizers]. Second, hyperpolarized markers typically have short signal lifetimes: typically, hyperpolarized signals may only be tracked for 1 to 2 min in the most favorable cases (*6*), greatly limiting this method as a probe for slower biological processes.

[1]Department of Chemistry, Duke University, Durham, NC 27708, USA. [2]Department of Physics, Duke University, Durham, NC 27708, USA. [3]Department of Mechanical Engineering and Materials Science, Duke University, Durham, NC 27708, USA. [4]Departments of Radiology and Biomedical Engineering, Vanderbilt University, Institute of Imaging Science, Nashville, TN 37232, USA. [5]Departments of Radiology and Biomedical Engineering, Duke University, Durham, NC 27708, USA.
*Corresponding author. E-mail: warren.warren@duke.edu (W.S.W.); qiu.wang@duke.edu (Q.W.); thomas.theis@duke.edu (T.T.)
†These authors contributed equally to this work.
‡Present address: Surbeck Laboratory of Advanced Imaging, Department of Radiology and Biomedical Imaging, University of California, San Francisco, San Francisco, CA 94158, USA.

The presented approach is inexpensive and produces long-lived signals

Here, we demonstrate that both of these challenges can be overcome simultaneously, setting the stage for hour-long tracking of molecular markers with inexpensive equipment. Specifically, we illustrate the potential of $^{15}N_2$-diazirines as uniquely powerful storage vessels for hyperpolarization. We show that diazirine can be hyperpolarized efficiently and rapidly (literally orders of magnitude cheaper and quicker than d-DNP), and that this hyperpolarization can be induced in states that maintain hyperpolarization for more than an hour.

Our approach uses parahydrogen (p-H_2) to directly polarize long-lived nuclear spin states. The first demonstration of parahydrogen-induced polarization (PHIP) was performed in the late 1980s (*17*–*19*). Then, PHIP was used to rely on the addition of p-H_2 to a carbon double or triple bond, incorporating highly polarized hydrogen atoms into molecules. This approach generally requires specific catalyst-substrate pairs; in addition, hydrogen atoms usually have short relaxation times (T_1) that cause signal decay within a few seconds. A more recent variant, SABRE (signal amplification by reversible exchange) (*20*, *21*), uses p-H_2 to polarize ^{1}H atoms on a substrate without hydrogenation. In SABRE, both p-H_2 and substrate reversibly bind to an iridium catalyst and the hyperpolarization is transferred from p-H_2 to the substrate through J-couplings established on the catalytic intermediate. Recently, we extended this method to SABRE-SHEATH (SABRE in SHield Enables Alignment Transfer to Heteronuclei) for direct hyperpolarization of ^{15}N molecular sites (*22*–*24*). This method has several notable features. Low-γ nuclei (^{13}C, ^{15}N) tend to have long relaxation times, particularly if a proton is not attached. In addition, conventional SABRE relies on small differences between four-bond proton-proton J-couplings (detailed in the Supplementary Materials), whereas SABRE-SHEATH uses larger two-bond heteronuclear J-couplings. It is extremely simple: SABRE-SHEATH requires nothing but p-H_2, the catalyst, and a shield to reduce Earth's field by about 99%. After 1 to 5 min of bubbling p-H_2 into the sample in the shield, we commonly achieve 10% nitrogen polarization, many thousands

of times stronger than thermal signals (*22*). In contrast, d-DNP typically produces such polarization levels in an hour, at much higher cost.

Diazirines are small and versatile molecular tags

A general strategy for many types of molecular imaging is the creation of molecular tags, which ideally do not alter biochemical pathways but provide background-free signatures for localization. This strategy has not been very successful in MR because of sensitivity issues. Here, we demonstrate that SABRE-SHEATH enables a MR molecular beacon strategy using diazirines $^{N}\!\!\diagup\!\!\diagdown^{N}$ (three-membered rings containing a nitrogen-nitrogen double bond). They are highly attractive as molecular tags, primarily because of their small size. Diazirines have already been established as biocompatible molecular tags for photoaffinity labeling (*25*). They can be incorporated into many small molecules, metabolites, and biomolecules without drastically altering biological function. Diazirines share similarities with methylene (CH_2) groups in terms of electronic and steric properties such that they can replace methylene groups without drastically distorting biochemical behavior. Furthermore, diazirines are stable at room temperature, are resistant to nucleophiles, and do not degrade under either acidic or alkaline conditions (*25*). With these attractive properties, diazirines have been used for the study of many signaling pathways. For example, they have been incorporated into hormones (*26*), epileptic drugs (*27*), antibiotics (*28*), hyperthermic drugs (*29*), anticancer agents (*30*), anesthetics (*31*), nucleic acids (*32*), amino acids (*33*), and lipids (*34*). They also have been introduced into specific molecular reporters to probe enzyme function and their binding sites such as in kinases (*35*), aspartic proteases (*36*), or metalloproteinases (*37*), to name a few. The nitrogen-nitrogen moiety is also intrinsically interesting, because the two atoms are usually very close in chemical shift and strongly coupled, thus suited to support a long-lived singlet state as described below.

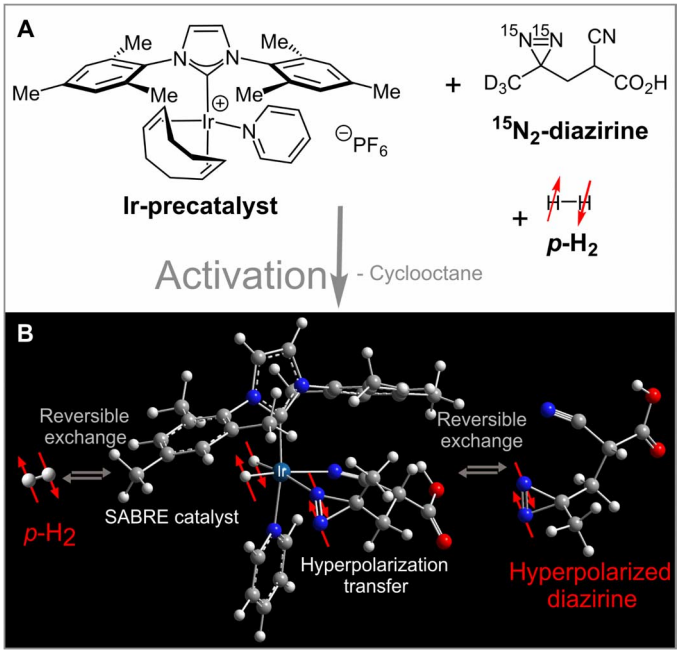

Fig. 1. The hyperpolarization mechanism. (**A**) The precatalyst, $^{15}N_2$-diazirine substrate, and *p*-H_2 are mixed, resulting in the activated species depicted in (B). (**B**) Both *p*-H_2 and the free $^{15}N_2$-diazirine [2-cyano-3-(D_3 methyl-$^{15}N_2$-diazirine)-propanoic acid] are in reversible exchange with the catalytically active iridium complex. The catalyst axial position is occupied by IMes [1,3-bis(2,4,6-trimethylphenyl)-imidazolium] and Py (pyridine) as nonexchanging ligands. The structure shown is a local energy minimum of the potential energy surface based on all-electron DFT calculations and the dispersion-corrected PBE density functional. In the complex, hyperpolarization is transferred from the parahydrogen (*p*-H_2)–derived hydrides to the ^{15}N nuclei (white, hydrogen; gray, carbon; blue, nitrogen; red, oxygen).

RESULTS AND DISCUSSION

Our first target molecule was 2-cyano-3-(D_3-methyl-$^{15}N_2$-diazirine)-propanoic acid in methanol-d_4, depicted in Fig. 1 along with the catalyst. To establish this hyperpolarization mode, we developed a new catalyst for this SABRE-SHEATH process. We synthesized [Ir(COD)(IMes)(Py)][PF_6] [COD, cyclooctadiene; IMes, 1,3-bis(2,4,6-trimethylphenyl)-imidazolium; Py, pyridine] as depicted in Fig. 1A. This precursor is dissolved in a diazirine-containing methanol solution and activated by bubbling

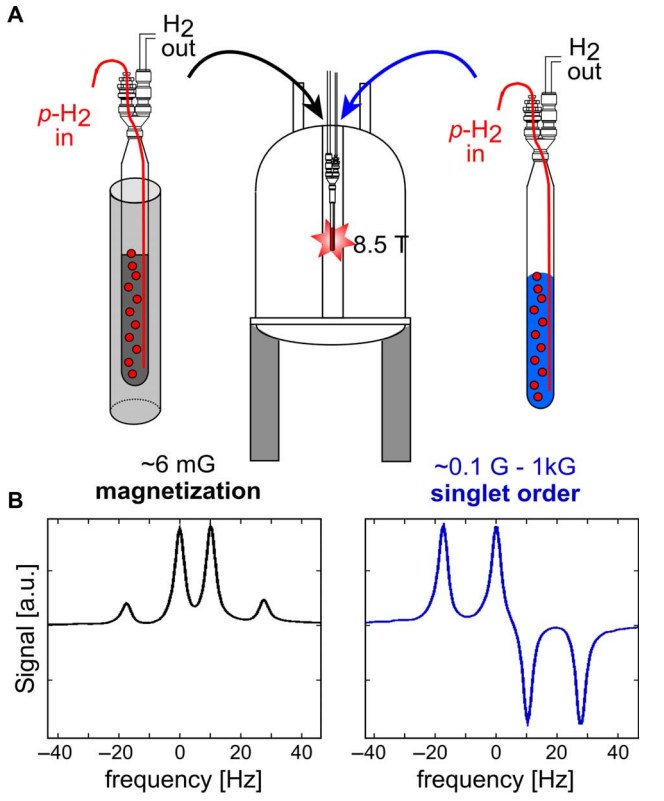

Fig. 2. Experimental and spectral distinction between magnetization and singlet spin order. (**A**) Experimental procedure. The sample is hyperpolarized by bubbling parahydrogen (*p*-H_2) through the solution in the NMR tube for 5 min and subsequently transferred into the high-field magnet for detection. If the hyperpolarization/bubbling is performed in a magnetic shield at ~6 mG, *z*-magnetization is created (black). If the hyperpolarization/bubbling is performed in the laboratory field anywhere between ~0.1 and ~1 kG, singlet order is created (blue). (**B**) *Z*-magnetization and singlet spin order can easily be distinguished based on their spectral appearance. a.u., arbitrary units. *Z*-magnetization produces an in-phase quartet (black). Singlet order gives an anti-phase quartet (blue). The spin system parameters for the $^{15}N_2$ two-spin system are J_{NN} = 17.3 Hz and $\Delta\delta$ = 0.58 parts per million.

hydrogen through this solution for ~20 min. This produces the catalytically active $[Ir(IMes)(H_2)(Py)(Diaz)]^+$ species depicted in Fig. 1B.

Density functional theory calculations shed light on polarization transfer catalyst

The Ir complex conformation shown in Fig. 1B was determined by all-electron density functional theory (DFT) calculations [semilocal Perdew-Burke-Ernzerhof (PBE) functional (*38*), corrected for long-range many-body dispersion interactions (*39*), in the FHI-aims software package (*40*, *41*); see the Supplementary Materials for details]. The calculations indicate a η^1 single-sided N attachment rather than η^2-N=N attachment of the diazirines. In the Ir complex, hyperpolarization is transferred from *p*-H_2 gas (~92% para-state, 7.5 atm) to the $^{15}N_2$-diazirine. Both *p*-H_2 and substrate are in reversible exchange with the central complex, which results in continuous pumping of hyperpolarization: *p*-H_2 is continually refreshed and hyperpolarization accumulated on the diazirine substrate.

An alternate polarization transfer catalyst is introduced

As opposed to the traditional [Ir(COD)(IMes)(Cl)] catalyst (*18*), the synthesized $[Ir(COD)(IMes)(Py)][PF_6]$ results in a pyridine ligand *trans* to IMes, improving our hyperpolarization levels by a factor of ~3 (see the Supplementary Materials). We have found that this new approach, which avoids competition from added pyridine, makes it possible to directly hyperpolarize a wide variety of different types of ^{15}N-containing molecules (and even ^{13}C). However, diazirines represent a particularly general and interesting class of ligands for molecular tags and are the focus here.

As depicted in Fig. 2A, the hyperpolarization proceeds outside the high-field NMR magnet at low magnetic fields, enabling SABRE-SHEATH directly targeting ^{15}N nuclei (*22*). To establish the hyperpolarization, we

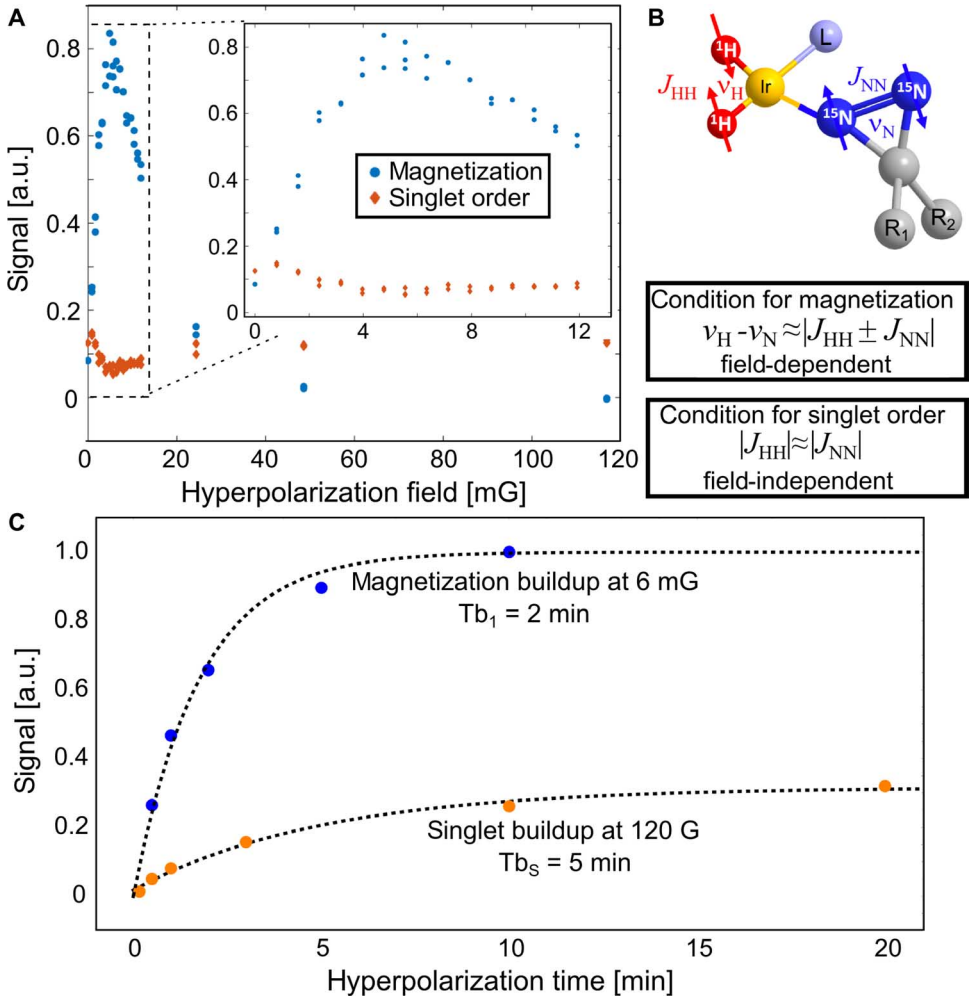

Fig. 3. Hyperpolarization buildup in the form of magnetization or singlet order. (**A**) Magnetization and singlet order as a function of magnetic field. The graph shows signal intensity after 5 min of bubbling. Magnetization is produced only at low magnetic fields inside the magnetic shield ideally at ~6 mG. Singlet order is obtained at any other magnetic field up to ~1 kG. (**B**) Spin systems and resonance conditions for forming magnetization versus singlet order. The condition for forming magnetization is field-dependent, whereas the condition for forming singlet order is not field-dependent, explaining the experimental observations of (A). (**C**) Polarization buildup as a function of bubbling time. Magnetization builds up faster, because the resonance condition can be matched exactly and T_1 is shorter, whereas singlet order builds up slower because the matching condition is not met exactly and T_S is longer. The measurements are performed with a methanol-d_4 solution containing 12 mM $^{15}N_2$-diazirine, 0.5 mM [IrCl(COD)(IMes)], 4 mM Py, and 960 mM D_2O.

bubble p-H_2 for ~5 min at the adequate field. Then, the sample is transferred into the NMR magnet within ~10 s, and $^{15}N_2$ signal detection is performed with a simple 90° pulse followed by data acquisition.

Two types of hyperpolarized states can be created: Magnetization and singlet order

We create two different types of hyperpolarization on the $^{15}N_2$-diazirine. We can hyperpolarize traditional z-magnetization, which corresponds to nuclear spins aligned with the applied magnetic field and is associated with pure in-phase signal as illustrated with the black trace in Fig. 2B. Alternatively, we can hyperpolarize singlet order on the $^{15}N_2$-diazirine, which corresponds to an anti-aligned spin state, with both spins pointing in opposite directions, entangled in a quantum mechanically "hidden" state. This hidden singlet order is converted into a detectable state when transferred to a high magnetic field and associated with the anti-phase signal illustrated by the blue trace in Fig. 2B (see the Supplementary Materials for details). The difference in symmetry of z-magnetization and singlet order leads to differences in signal decay rates; z-magnetization is directly exposed to all NMR relaxation mechanisms and is often associated with shorter signal lifetimes, which may impede molecular tracking on biologically relevant time scales. Singlet order, on the other hand, is protected from many relaxation mechanisms because it has

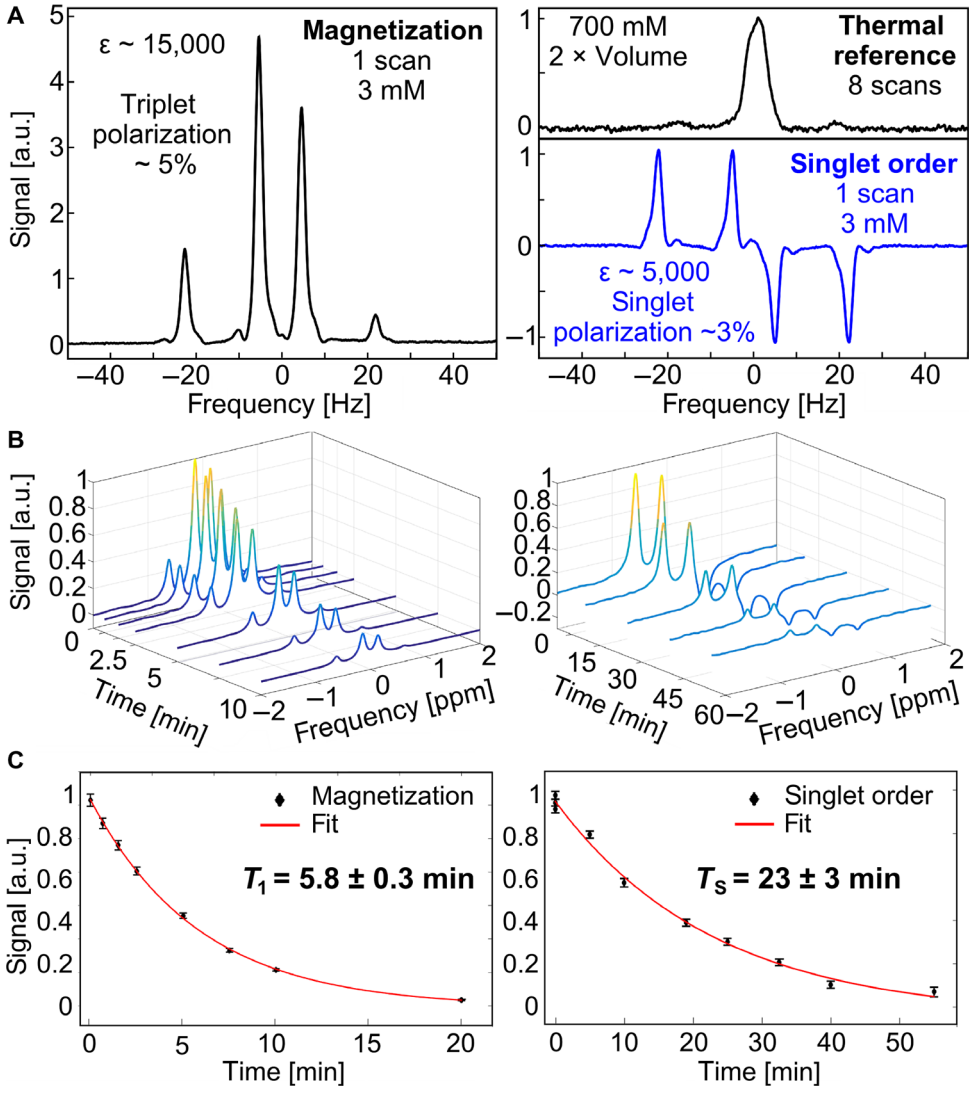

Fig. 4. Maximum enhancement levels and decay time constants observed for magnetization and singlet order. (**A**) Single-shot SABRE-SHEATH spectra obtained from a methanol-d_4 solution containing 3 mM $^{15}N_2$-diazirine, 0.125 mM [Ir(COD)(IMes)(Py)][PF_6], and 240 mM D_2O. Enhancements are obtained by comparison to the displayed thermal reference spectrum of the $^{15}N_2$-diazirine [2-cyano-3-(D_3-methyl-$^{15}N_2$-diazirine)-propanoic acid] in D_2O. (In D_2O, the chemical shift difference between the ^{15}N nuclei is smaller than that in MeOH, and therefore, only one peak is observed.) (**B**) Representative T_1 and T_S decay measurements. T_1 is measured at 120 G (12 mT) from a methanol-d_4 solution containing 12 mM $^{15}N_2$-diazirine, 0.125 mM [IrCl(COD)(IMes)], 1 mM Py, and 960 mM D_2O. T_S is measured at 3 G (0.3 mT) from a solution containing 12 mM $^{15}N_2$-diazirine, 0.05 mM [IrCl(COD)(IMes)], and 0.4 mM Py. (**C**) The z-magnetization and singlet-order components are extracted from the data sets in (B) and fit to a single exponential (see the Supplementary Materials for further details).

no angular momentum (*42*–*52*) and can therefore exhibit much longer lifetimes, enabling hour-long molecular tracking.

The type of hyperpolarized state is selected by the magnetic field

We can control which type of hyperpolarization we create by choosing the appropriate magnetic fields for the bubbling process. *Z*-magnetization is created in the SABRE-SHEATH mode at low magnetic fields inside a magnetic shield (*22*–*24*, *53*, *54*). This behavior is explained by resonance conditions for hyperpolarizing magnetization versus singlet order that we derive in the Supplementary Materials. The condition for creating magnetization, $\nu_H - \nu_N = |J_{HH} \pm J_{NN}|$, is field-dependent in the NMR frequencies, ν_H and ν_N, and field-independent in the *J*-couplings. Accordingly, hyperpolarized magnetization is created at a magnetic field where the frequency difference matches the *J*-couplings. This magnetic field is ~6 mG, which is obtained by using $J_{HH} = -10$ Hz, $J_{NN} = -17.3$ Hz, $\gamma_{1H} = 4.2576$ kHz/G, and $\gamma_{15N} = -0.4316$ kHz/G (see the Supplementary Materials). The theoretical prediction of 6 mG matches the experimental maximum for hyperpolarized *z*-magnetization illustrated by the blue data in Fig. 3A.

The condition for creating singlet order, on the other hand, $J_{HH} = \pm J_{NN}$, is not dependent on the magnetic field and, for the system at hand, is fulfilled closely enough ($J_{HH} \sim 10$ Hz, $J_{NN} \sim -17.3$ Hz) such that singlet order can be induced virtually at any magnetic field, under the condition that the singlet state remains close to an eigenstate of the Hamiltonian, which is true for fields up to ~1 kG. As illustrated in Fig. 3C, the singlet buildup is indeed slightly slower and less efficient, as expected for an imperfectly matched resonance condition. Accordingly, the optimal magnetic field for hyperpolarizing singlet order is not tied to specific magnetic fields. Instead, the optimal magnetic field to produce singlet order is the field associated with the longest singlet lifetime, allowing for accumulation over a long time span. We find well-suited lifetimes at fields between ~0.5 and ~200 G.

Central results: 5% polarization for magnetization with 6-min decay constant, 3% singlet polarization with 23-min decay constant

For *z*-magnetization, we observe up to 15,000-fold signal enhancements over thermal control experiments at 8.5 T displayed in Fig. 4A. This corresponds to ~5% polarization. For singlet order, up to 5000-fold signal enhancements are observed, corresponding to ~3% singlet polarization. Notice that the singlet polarization level is not much lower than the polarization of magnetization despite the signal enhancement being three times lower. This mismatch between enhancements and polarization is attributed to the singlet readout being ~60% as efficient as the magnetization readout in our current setup (see the Supplementary Materials). Figure 4 (B and C) displays typical T_1 and T_S lifetime measurements. Spectra are obtained after 5-min bubbling and a varying relaxation delay at a chosen holding field. The acquired spectra are subsequently integrated and fit to mono-exponential decays shown in Fig. 4C. Under conditions of relatively low catalyst concentrations and relatively low magnetic fields, as specified in the figure caption, a T_1 of 5.8 ± 0.3 min and a T_S of 23 ± 3 min are observed (see the Supplementary Materials for more exhaustive data under various concentrations and magnetic fields). Typical ^{13}C hyperpolarization studies collect data for about three times the spin lifetime, which is about 3 min (3×1 min) for typical ^{13}C substrates. Here, the 23-min lifetime enables data collection for over an hour.

CONCLUSION

The demonstrated hyperpolarization lifetimes, combined with the ease of hyperpolarization in these broadly applicable biomolecular tags, may establish a paradigm shift for biomolecular sensing and reporting in optically opaque tissue. The demonstrated lifetimes even exceed lifetimes of some common radioactive tracers used in positron emission tomography (PET) (for example, ^{11}C, 20.3 min). However, unlike PET, MR is exquisitely sensitive to chemical transformations and does not use ionizing radiation (such that, for example, daily progression monitoring of disease is easily possible). The presented work may allow direct access to biochemical mechanisms and kinetics in optically opaque media. We therefore envision tracking subtle biochemical processes in vitro with unprecedented NMR sensitivities as well as real-time in vivo biomolecular imaging with hyperpolarized diazirines.

MATERIALS AND METHODS

Samples hyperpolarized with [Ir(COD)(IMes)(Py)][PF_6] as precursor

We prepared a stock solution of 0.5 M [Ir(COD)(IMes)(Py)][PF_6] in CD_3OD. Subsequently, an appropriate aliquot of this stock solution was added into the NMR tube containing CD_3OD such that a volume of 600 µl of the targeted concentration was obtained. To this solution, we then added an aliquot of a 700 mM solution of the diazirine in D_2O to achieve the desired diazirine concentration.

Samples hyperpolarized with [Ir(COD)(IMes)Cl] as precursor

We prepared a stock solution of 0.5 M [Ir(COD)(IMes)Cl] plus 8 eq of pyridine, that is, 4 M in CD_3OD. Subsequently, an appropriate aliquot of this stock solution was added into the NMR tube containing CD3OD such that a volume of 600 µl at the targeted concentration was obtained. To this solution, we then added an aliquot of a 700 mM solution of the diazirine in D_2O to achieve the desired diazirine concentration.

Parahydrogen production

Parahydrogen (p-H_2) gas (~92% para-state, 8.2 atm) was created in a Bruker parahydrogen generator (slightly modified to access higher pressures) and bubbled through the solution prepared above. For catalyst activation, bubbling was performed for 20 min before starting any experiments.

Experimental setup to obtain well-controlled milligauss fields

A set of three layers of magnetic shielding was used to obtain a low–magnetic field environment (MuMETAL Zero Gauss Chambers; product ZG-206, Magnetic Shield Corp.) The shields are degaussed with a degaussing coil wrapped around the innermost shield. In the center of the shields, we placed a solenoid with length $L = 47.5$ cm and $N = 165$ turns (see the Supplementary Materials for further details and a picture).

SUPPLEMENTARY MATERIALS

Supplementary material for this article is available at http://advances.sciencemag.org/cgi/content/full/2/3/e1501438/DC1

Synthesis of $^{15}N_2$-diazirine and iridium precatalyst

REFERENCES AND NOTES

1. J. H. Ardenkjær-Larsen, B. Fridlund, A. Gram, G. Hansson, L. Hansson, M. H. Lerche, R. Servin, M. Thaning, K. Golman, Increase in signal-to-noise ratio of > 10,000 times in liquid-state NMR. *Proc. Natl. Acad. Sci. U.S.A.* **100**, 10158–10163 (2003).
2. A. Gottberg, M. Stachura, M. Kowalska, M. L. Bissell, V. Arcisauskaite, K. Blaum, A. Helmke, K. Johnston, K. Kreim, F. H. Larsen, R. Neugart, G. Neyens, R. F. Garcia Ruiz, D. Szunyogh, P. W. Thulstrup, D. T. Yordanov, L. Hemmingsen, Billion-fold enhancement in sensitivity of nuclear magnetic resonance spectroscopy for magnesium ions in solution. *Chem. Phys. Chem.* **15**, 3929–3932 (2014).
3. R. V. Shchepin, A. M. Coffey, K. W. Waddell, E. Y. Chekmenev, Parahydrogen induced polarization of 1-^{13}C-phospholactate-d_2 for biomedical imaging with > 30,000,000-fold NMR signal enhancement in water. *Anal. Chem.* **86**, 5601–5605 (2014).
4. T. B. Rodrigues, E. M. Serrao, B. W. C. Kennedy, D.-E. Hu, M. I. Kettunen, K. M. Brindle, Magnetic resonance imaging of tumor glycolysis using hyperpolarized ^{13}C-labeled glucose. *Nat. Med.* **20**, 93–97 (2014).
5. K. R. Keshari, D. M. Wilson, Chemistry and biochemistry of ^{13}C hyperpolarized magnetic resonance using dynamic nuclear polarization. *Chem. Soc. Rev.* **43**, 1627–1659 (2014).
6. S. J. Nelson, J. Kurhanewicz, D. B. Vigneron, P. E. Z. Larson, A. L. Harzstark, M. Ferrone, M. van Criekinge, J. W. Chang, R. Bok, I. Park, G. Reed, L. Carvajal, E. J. Small, P. Munster, V. K. Weinberg, J. H. Ardenkjaer-Larsen, A. P. Chen, R. E. Hurd, L.-I. Odegardstuen, F. J. Robb, J. Tropp, J. A. Murray, Metabolic imaging of patients with prostate cancer using hyperpolarized [1-^{13}C]-pyruvate. *Sci. Transl. Med.* **5**, 198ra108 (2013).
7. J. Kurhanewicz, D. B. Vigneron, K. Brindle, E. Y. Chekmenev, A. Comment, C. H. Cunningham, R. J. DeBerardinis, G. G. Green, M. O. Leach, S. S. Rajan, R. R. Rizi, B. D. Ross, W. S. Warren, C. R. Malloy, Analysis of cancer metabolism by imaging hyperpolarized nuclei: Prospects for translation to clinical research. *Neoplasia* **13**, 81–97 (2011).
8. R. Aggarwal, J. Kurhanewicz, Prostate cancer in 2013: The changing role of imaging in clinical care. *Nat. Rev. Urol.* **11**, 75–77 (2014).
9. Y. Li, I. Park, S. J. Nelson, Imaging tumor metabolism using in vivo magnetic resonance spectroscopy. *Cancer J.* **21**, 123–128 (2015).
10. K. G. Valentine, G. Mathies, S. Bédard, N. V. Nucci, I. Dodevski, M. A. Stetz, T. V. Can, R. G. Griffin, A. J. Wand, Reverse micelles as a platform for dynamic nuclear polarization in solution NMR of proteins. *J. Am. Chem. Soc.* **136**, 2800–2807 (2014).
11. H.-Y. Chen, M. Ragavan, C. Hilty, Protein folding studied by dissolution dynamic nuclear polarization. *Angew. Chem. Int. Ed.* **52**, 9192–9195 (2013).
12. A. N. Smith, M. A. Caporini, G. E. Fanucci, J. R. Long, A method for dynamic nuclear polarization enhancement of membrane proteins. *Angew. Chem. Int. Ed.* **54**, 1542–1546 (2015).
13. A. Bornet, X. Ji, D. Mammoli, B. Vuichoud, J. Milani, G. Bodenhausen, S. Jannin, Long-lived states of magnetically equivalent spins populated by dissolution-DNP and revealed by enzymatic reactions. *Chem. Eur. J.* **20**, 17113–17118 (2014).
14. Q. Chappuis, J. Milani, B. Vuichoud, A. Bornet, A. D. Gossert, G. Bodenhausen, S. Jannin, Hyperpolarized water to study protein–ligand interactions. *J. Phys. Chem. Lett.* **6**, 1674–1678 (2015).
15. Ü. Akbey, W. T. Franks, A. Linden, S. Lange, R. G. Griffin, B.-J. van Rossum, H. Oschkinat, Dynamic nuclear polarization of deuterated proteins. *Angew. Chem. Int. Ed.* **49**, 7803–7806 (2010).
16. Y. Kim, C. Hilty, Affinity screening using competitive binding with fluorine-19 hyperpolarized ligands. *Angew. Chem. Int. Ed.* **54**, 4941–4944 (2015).
17. C. R. Bowers, D. P. Weitekamp, Transformation of symmetrization order to nuclear-spin magnetization by chemical reaction and nuclear magnetic resonance. *Phys. Rev. Lett.* **57**, 2645–2648 (1986).
18. C. R. Bowers, D. P. Weitekamp, Parahydrogen and synthesis allow dramatically enhanced nuclear alignment. *J. Am. Chem. Soc.* **109**, 5541–5542 (1987).
19. T. C. Eisenschmid, R. U. Kirss, P. P. Deutsch, S. I. Hommeltoft, R. Eisenberg, J. Bargon, R. G. Lawler, A. L. Balch, Para hydrogen induced polarization in hydrogenation reactions. *J. Am. Chem. Soc.* **109**, 8089–8091 (1987).
20. R. W. Adams, J. A. Aguilar, K. D. Atkinson, M. J. Cowley, P. I. P. Elliott, S. B. Duckett, G. G. R. Green, I. G. Khazal, J. López-Serrano, D. C. Williamson, Reversible interactions with para-hydrogen enhance NMR sensitivity by polarization transfer. *Science* **323**, 1708–1711 (2009).
21. M. J. Cowley, R. W. Adams, K. D. Atkinson, M. C. R. Cockett, S. B. Duckett, G.G. R. Green, J. A. B. Lohman, R. Kerssebaum, D. Kilgour, R. E. Mewis, Iridium N-heterocyclic carbene complexes as efficient catalysts for magnetization transfer from para-hydrogen. *J. Am. Chem. Soc.* **133**, 6134–6137 (2011).
22. T. Theis, M. L. Truong, A. M. Coffey, R. V. Shchepin, K. W. Waddell, F. Shi, B. M. Goodson, W. S. Warren, E. Y. Chekmenev, Microtesla SABRE enables 10% nitrogen-15 nuclear spin polarization. *J. Am. Chem. Soc.* **137**, 1404–1407 (2015).
23. R. V. Shchepin, M. L. Truong, T. Theis, A. M. Coffey, F. Shi, K. W. Waddell, W. S. Warren, B. M. Goodson, E. Y. Chekmenev, Hyperpolarization of "neat" liquids by NMR signal amplification by reversible exchange. *J. Chem. Phys. Lett.* **6**, 1961–1967 (2015).
24. M. L. Truong, T. Theis, A. M. Coffey, R. V. Shchepin, K. W. Waddell, F. Shi, B. M. Goodson, W. S. Warren, E. Y. Chekmenev, ^{15}N hyperpolarization by reversible exchange using SABRE-SHEATH. *J. Phys. Chem. C* **119**, 8786–8797 (2015).
25. L. Dubinsky, B. P. Krom, M. M. Meijler, Diazirine based photoaffinity labeling. *Bioorg. Med. Chem.* **20**, 554–570 (2012).
26. T. Kinoshita, A. Caño-Delgado, H. Seto, S. Hiranuma, S. Fujioka, S. Yoshida, J. Chory, Binding of brassinosteroids to the extracellular domain of plant receptor kinase BRI1. *Nature* **433**, 167–171 (2005).
27. Y. Wang, K. D. Park, C. Salomé, S. M. Wilson, J. P. Stables, R. Liu, R. Khanna, H. Kohn, Development and characterization of novel derivatives of the antiepileptic drug lacosamide that exhibit far greater enhancement in slow inactivation of voltage-gated sodium channels. *ACS Chem. Neurosci.* **2**, 90–106 (2011).
28. D. Riber, M. Venkataramana, S. Sanyal, T. Duvold, Synthesis and biological evaluation of photoaffinity labeled fusidic acid analogues. *J. Med. Chem.* **49**, 1503–1505 (2006).
29. T. Hosoya, T. Hiramatsu, T. Ikemoto, H. Aoyama, T. Ohmae, M. Endo, M. Suzuki, Design of dantrolene-derived probes for radioisotope-free photoaffinity labeling of proteins involved in the physiological Ca^{2+} release from sarcoplasmic reticulum of skeletal muscle. *Bioorg. Med. Chem. Lett.* **15**, 1289–1294 (2005).
30. L. Luo, C. A. Parrish, N. Nevins, D. E. McNulty, A. M. Chaudhari, J. D. Carson, V. Sudakin, A. N. Shaw, R. Lehr, H. Zhao, S. Sweitzer, L. Lad, K. W. Wood, R. Sakowicz, R. S. Annan, P. S. Huang, J. R. Jackson, D. Dhanak, R. A. Copeland, K. R. Auger, ATP-competitive inhibitors of the mitotic kinesin KSP that function via an allosteric mechanism. *Nat. Chem. Biol.* **3**, 722–726 (2007).
31. M. A. Hall, J. Xi, C. Lor, S. Dai, R. Pearce, W. P. Dailey, R. G. Eckenhoff, *m*-Azipropofol (AziP*m*) a photoactive analogue of the intravenous general anesthetic propofol. *J. Med. Chem.* **53**, 5667–5675 (2010).
32. M. Liebmann, F. Di Pasquale, A. Marx, A new photoactive building block for investigation of DNA backbone interactions: Photoaffinity labeling of human DNA polymerase β. *ChemBioChem* **7**, 1965–1969 (2006).
33. M. Suchanek, A. Radzikowska, C. Thiele, Photo-leucine and photo-methionine allow identification of protein-protein interactions in living cells. *Nat. Methods* **2**, 261–268 (2005).
34. M. Hashimoto, Y. Hatanaka, A novel biotinylated diazirinyl ceramide analogue for photoaffinity labeling. *Bioorg. Med. Chem. Lett.* **18**, 650–652 (2008).
35. M. Kaneda, S. Masuda, T. Tomohiro, Y. Hatanaka, A simple and efficient photoaffinity method for proteomics of GTP-binding proteins. *ChemBioChem* **8**, 595–598 (2007).

36. H. Fuwa, Y. Takahashi, Y. Konno, N. Watanabe, H. Miyashita, M. Sasaki, H. Natsugari, T. Kan, T. Fukuyama, T. Tomita, T. Iwatsubo, Divergent synthesis of multifunctional molecular probes to elucidate the enzyme specificity of dipeptidic γ-secretase inhibitors. *ACS Chem. Biol.* **2**, 408–418 (2007).
37. E. W. S. Chan, S. Chattopadhaya, R. C. Panicker, X. Huang, S. Q. Yao, Developing photoactive affinity probes for proteomic profiling: Hydroxamate-based probes for metalloproteases. *J. Am. Chem. Soc.* **126**, 14435–14446 (2004).
38. J. P. Perdew, K. Burke, M. Ernzerhof, Generalized gradient approximation made simple. *Phys. Rev. Lett.* **77**, 3865–3868 (1996).
39. A. Ambrosetti, A. M. Reilly, R. A. DiStasio Jr., A. Tkatchenko, Long-range correlation energy calculated from coupled atomic response functions. *J. Chem. Phys.* **140**, 18A508 (2014).
40. V. Blum, R. Gehrke, F. Hanke, P. Havu, V. Havu, X. Ren, K. Reuter, M. Scheffler, *Ab initio* molecular simulations with numeric atom-centered orbitals. *Comput. Phys. Commun.* **180**, 2175–2196 (2009).
41. V. Havu, V. Blum, P. Havu, M. Scheffler, Efficient O(N) integration for all-electron electronic structure calculation using numeric basis functions. *J. Comput. Phys.* **228**, 8367–8379 (2009).
42. M. Carravetta, M. H. Levitt, Long-lived nuclear spin states in high-field solution NMR. *J. Am. Chem. Soc.* **126**, 6228–6229 (2004).
43. M. Carravetta, O. G. Johannessen, M. H. Levitt, Beyond the T_1 limit: Singlet nuclear spin states in low magnetic fields. *Phys. Rev. Lett.* **92**, 153003 (2004).
44. W. S. Warren, E. Jenista, R. T. Branca, X. Chen, Increasing hyperpolarized spin lifetimes through true singlet eigenstates. *Science* **323**, 1711–1714 (2009).
45. G. Pileio, M. Carravetta, E. Hughes, M. H. Levitt, The long-lived nuclear singlet state of ^{15}N-nitrous oxide in solution. *J. Am. Chem. Soc.* **130**, 12582–12583 (2008).
46. M. H. Levitt, Singlet nuclear magnetic resonance. *Annu. Rev. Phys. Chem.* **63**, 89–105 (2012).
47. V. V. Zhivonitko, K. V. Kovtunov, P. L. Chapovsky, I. V. Koptyug, Nuclear spin isomers of ethylene: Enrichment by chemical synthesis and application for NMR signal enhancement. *Angew. Chem. Int. Ed. Engl.* **52**, 13251–13255 (2013).
48. M. B. Franzoni, L. Buljubasich, H. W. Spiess, K. Munnemann, Long-lived ^{1}H singlet spin states originating from para-hydrogen in Cs-symmetric molecules stored for minutes in high magnetic fields. *J. Am. Chem. Soc.* **134**, 10393–10396 (2012).
49. Y. Zhang, P. C. Soon, A. Jerschow, J. W. Canary, Long-lived ^{1}H nuclear spin singlet in dimethyl maleate revealed by addition of thiols. *Angew. Chem. Int. Ed. Engl.* **53**, 3396–3399 (2014).
50. G. Stevanato, J. T. Hill-Cousins, P. Håkansson, S. S. Roy, L. J. Brown, R. C. Brown, G. Pileio, M. H. Levitt, A nuclear singlet lifetime of more than one hour in room-temperature solution. *Angew. Chem. Int. Ed. Engl.* **54**, 3740–3743 (2015).
51. D. Canet, S. Bouguet-Bonnet, C. Aroulanda, F. Reineri, About long-lived nuclear spin states involved in para-hydrogenated molecules. *J. Am. Chem. Soc.* **129**, 1445–1449 (2007).
52. T. Jonischkeit, U. Bommerich, J. Stadler, K. Woelk, H. G. Niessen, J. Bargon, Generating long-lasting ^{1}H and ^{13}C hyperpolarization in small molecules with parahydrogen-induced polarization. *J. Chem. Phys.* **124**, 201109 (2006).
53. T. Theis, M. P. Ledbetter, G. Kervern, J. W. Blanchard, P. J. Ganssle, M. C. Butler, H. D. Shin, D. Budker, A. Pines, Zero-field NMR enhanced by parahydrogen in reversible exchange. *J. Am. Chem. Soc.* **134**, 3987–3990 (2012).
54. T. Theis, P. Ganssle, G. Kervern, S. Knappe, J. Kitching, M. P. Ledbetter, D. Budker, A. Pines, Parahydrogen-enhanced zero-field nuclear magnetic resonance. *Nat. Phys.* **7**, 571–575 (2011).
55. M. W. Rathke, A. A. Millard, Boranes in functionalization of olefins to amines: 3-Pinanamine [bicyclo[3.1.1]heptan-3-amine, 2,6,6-trimethyl-]. *Org. Synth.* **58**, 32 (1978).
56. A. D. Rodriguez, A. Nickon, A convenient synthesis of vinyl sulfides. *Tetrahedron* **41**, 4443–4448 (1985).
57. A. E. Davey, A. F. Parsons, R. J. K. Taylor, Reactions of dithiane derived alcohols: Promotion of the Thorpe-Ingold effect by trimethylsilyl and t-butyl substituents. *J. Chem. Soc., Perkin Trans.* **1**, 1853–1858 (1989).
58. R. F. R. Church, M. J. Weiss, Diazirines. II. Synthesis and properties of small functionalized diazirine molecules. Observations on the reaction of a diaziridine with the iodine-iodide ion system. *J. Org. Chem.* **35**, 2465–2471 (1970).
59. S. E. Franz, R. R. Watkins, L. A. Wright, B. A. Weaver, R. C. Hartage, I. Ghiviriga, G. Gumina, B. D. Feske, Synthetic strategy toward γ-keto nitriles and their biocatalytic conversion to asymmetric γ-lactones. *Synthesis* **45**, 2171–2178 (2013).
60. F. Burel, J.-P. Couvercelle, C. Bunel, J.-M. Saiter, Poly-α-*n*-alkyl acrylic derivatives: Synthesis, influence of molecuur weight and *n*-alkyl group length on physical and physicochemical properties. *J. Macromol. Sci. Part A* **32**, 1091–1102 (1995).
61. A. C. Hillier, H. M. Lee, E. D. Stevens, S. P. Nolan, Cationic iridium complexes bearing imidazol-2-ylidene ligands as transfer hydrogenation catalysts. *Organometallics* **20**, 4246–4252 (2001).
62. M. C. D. Tayler, M. H. Levitt, Singlet nuclear magnetic resonance of nearly-equivalent spins. *Phys. Chem. Chem. Phys.* **13**, 5556–5560 (2011).
63. S. J. DeVience, R. L. Walsworth, M. S. Rosen, Preparation of nuclear spin singlet states using spin-lock induced crossing. *Phys. Rev. Lett.* **111**, 173002 (2013).
64. T. Theis, Y. Feng, T. Wu, W. S. Warren, Composite and shaped pulses for efficient and robust pumping of disconnected eigenstates in magnetic resonance. *J. Chem. Phys.* **140**, 014201 (2014).
65. S. Chutia, M. Rossi, V. Blum, Water adsorption at two unsolvated peptides with a protonated lysine residue: From self-solvation to solvation. *J. Phys. Chem. B* **116**, 14788–14804 (2012).
66. M. Rossi, S. Chutia, M. Scheffler, V. Blum, Validation challenge of density-functional theory for peptides—Example of Ac-Phe-Ala$_5$-LysH$^+$. *J. Phys. Chem. A* **118**, 7349–7359 (2014).
67. F. Schubert, M. Rossi, C. Baldauf, K. Pagel, S. Warnke, G. von Helden, F. Filsinger, P. Kupser, G. Meijer, M. Salwiczek, B. Koksch, M. Scheffler, V. Blum, Exploring the conformational preferences of 20-residue peptides in isolation: Ac-Ala$_{19}$-Lys + H$^+$ *vs.* Ac-Lys-Ala$_{19}$ + H$^+$ and the current reach of DFT. *Phys. Chem. Chem. Phys.* **17**, 7373–7385 (2015).
68. A. Tkatchenko, M. Scheffler, Accurate molecular van der Waals interactions from ground-state electron density and free-atom reference data. *Phys. Rev. Lett.* **102**, 073005 (2009).
69. J. Antonio Jimenez, R. M. Claramunt, O. Mó, M. Yáñez, F. Wehrmann, G. Buntkowsky, H.-H. Limbach, R. Goddard, J. Elguero, The structure of *N*-aminopyrazole in the solid state and in solution: An experimental and computational study. *Phys. Chem. Chem. Phys.* **1**, 5113–5120 (1999).

Funding: This work was supported by NSF grants CHE-1058727, CHE-1363008, and CHE-1416268; NIH grant 1R21EB018014; and Department of Defense Congressionally Directed Medical Research Programs Breast Cancer grant W81XWH-12-1-0159/BC112431. W.P.H., T.T., V.B., and W.S.W. also acknowledge funding from a Pratt School of Engineering Research Innovation Seed Fund Grant. Q.W. and S.J.M. acknowledge support from Duke University. G.X.O. also acknowledges support from the Burroughs Wellcome Fellowship. Furthermore, acknowledgment is made to the Donors of the American Chemical Society Petroleum Research Fund for partial support of this research. **Author contributions:** T.T. envisioned direct hyperpolarization of long-lived states with SABRE, designed experiments, conducted experiments, analyzed data, developed spin dynamics theory, and wrote the manuscript. G.X.O. designed and synthesized $^{15}N_2$-diazirine molecules, conducted initial characterization, and edited the manuscript. A.W.J.L. conceived and synthesized SABRE catalysts, edited the manuscript, and conducted most of the experiments. K.E.C. analyzed data, developed spin dynamics theory, and assisted with experiments. Y.F. envisioned $^{15}N_2$-diazirine as storage vessels for long-lived hyperpolarization and conducted initial characterization. W.P.H. designed and conducted all-electron DFT simulations. V.B. designed and advised on the all-electron DFT simulations. S.J.M. conceived and advised on the synthesis of the SABRE precatalysts and edited the manuscript. E.Y.C. advised on the experimental design and edited the manuscript. Q.W. envisioned $^{15}N_2$-diazirine as a general tag for MRI molecular labeling; advised on experimental design, initial characterization, and synthesis of $^{15}N_2$-diazirine; and edited the manuscript. W.S.W. envisioned $^{15}N_2$-diazirine as storage vessels for long-lived hyperpolarization, advised on experimental design and development of spin dynamics theory, and edited the manuscript. **Competing interests:** The authors declare that they have no competing interests. **Data and materials availability:** All data needed to evaluate the conclusions in the paper are present in the paper and/or the Supplementary Materials. Additional data are available from the authors upon request.

Submitted 12 October 2015
Accepted 5 February 2016
Published 25 March 2016
10.1126/sciadv.1501438

Citation: T. Theis, G. X. Ortiz Jr., A. W. J. Logan, K. E. Claytor, Y. Feng, W. P. Huhn, V. Blum, S. J. Malcolmson, E. Y. Chekmenev, Q. Wang, W. S. Warren, Direct and cost-efficient hyperpolarization of long-lived nuclear spin states on universal $^{15}N_2$-diazirine molecular tags. *Sci. Adv.* **2**, e1501438 (2016).